Journal of Materials Chemistry A

ROYAL SOCIETY OF CHEMISTRY

PAPER

View Article Online
View Journal | View Issue

Cite this: J. Mater. Chem. A, 2023, 11, 14768

A polymer acceptor with grafted small molecule acceptor units for high-efficiency organic solar cells†

Yuzhong Huang,‡[a] Xiaodong Si,‡[a] Ruohan Wang,[a] Kangqiao Ma,[a] Wendi Shi,[a] Changzun Jiang,[a] Yan Lu,*[b] Chenxi Li,[a] Xiangjian Wan*[a] and Yongsheng Chen*[a]

Received 27th April 2023
Accepted 7th June 2023

DOI: 10.1039/d3ta02523c

rsc.li/materials-a

Polymerization of small molecule acceptors (SMAs) has been proved to be an effective strategy to design polymer acceptors, in which the polymerization reaction is conducted *via* the coupling between the end groups of SMAs and linkers. However, polymer acceptors synthesized in this polymerization way cannot remain the favored packing modes of end groups in the original SMAs. Herein, we propose a strategy for designing polymer acceptors with grafted SMA units *via* the polymerization between central building blocks of SMAs and linkers. Polymer acceptors designed using this strategy can not only free the end groups to facilitate effective packing similar to SMAs but also form extended conjugation and double charge transport channels. With this strategy, a polymer acceptor **SH-1** was synthesized, which shows more compact and ordered intermolecular packing in both neat and blended films compared with the corresponding **SH-2** synthesized by conventional copolymerization *via* end groups and linkers. The all-polymer solar cells based on PM6:**SH-1** showed a power conversion efficiency (PCE) of 14.14%, substantially higher than that of the PM6:**SH-2** based device with an efficiency of 6.55%. This work provides a new strategy for designing polymer acceptors with great potential through further careful regulation of both main building blocks and linker groups.

1. Introduction

In the past decades, organic solar cells (OSCs) have made great progress through intensive efforts in material design, device optimization and mechanism investigation.[1–8] Recently, benefiting from the emergence of the acceptor–donor–acceptor (A–D–A)-type small-molecule acceptors (SMAs),[9] particularly the Y-series acceptors, OSCs based on polymer donors and SMAs have realized power conversion efficiencies (PCEs) over 19%.[10–15] In comparison with SMA-based OSCs, all-polymer solar cells (all-PSCs) with polymers as both donors and acceptors have their unique merits, *e.g.*, good thermal and morphological stability, excellent stretchability and mechanical durability.[16–19] Currently, PCEs exceeding 18% have been achieved for all-PSCs[8,20–24] mainly attributed to the innovation of polymer acceptor materials, especially polymer acceptors designed with the SMA-polymerization strategy proposed by Li *et al.*[18,25] To date, SMA-polymerization has proved to be an effective and successful strategy to design polymer acceptors and the majority of high-performance polymer acceptors are constructed by polymerizing A–D–A type acceptors such as ITIC and Y-series SMAs.[21,26–30] However, as shown in Fig. 1a, the polymerization reaction sites in the above reported polymer acceptors are all located at the electron-deficient end groups. Polymer acceptors copolymerized *via* the end groups of SMAs and linkers might have several inherent issues. (1) Decreased intermolecular packing interaction: the intermolecular packing between electron withdrawing end groups has proved to be an essential and crucial packing mode in non-fullerene SMAs, which benefits the formation of efficient charge transport channels.[31–33] However, after polymerizing with other linkers, the packing mode of the end groups in the original SMAs will be significantly changed. Especially, in many cases, the skeleton planarity of the polymer acceptors cannot be ensured owing to the twist conformation between the end groups of SMAs and the linker units, which will also be unfavourable for the intermolecular packing and corresponding device photovoltaic performances.[26,34] (2) Reduced electron-deficient property of the end groups: with the polymerization between the end groups and linkers, the electron-

[a]State Key Laboratory of Elemento-Organic Chemistry, The Centre of Nanoscale Science and Technology, Key Laboratory of Functional Polymer Materials, College of Chemistry, Renewable Energy Conversion and Storage Center (RECAST), Nankai University, Tianjin 300071, China. E-mail: xjwan@nankai.edu.cn; yschen99@nankai.edu.cn

[b]School of Materials Science & Engineering, Key Laboratory of Display Materials & Photoelectric Devices, Ministry of Education, Tianjin University of Technology, Tianjin 300384, China. E-mail: luyan@tjut.edu.cn

† Electronic supplementary information (ESI) available. See DOI: https://doi.org/10.1039/d3ta02523c

‡ These authors contributed equally to this work.

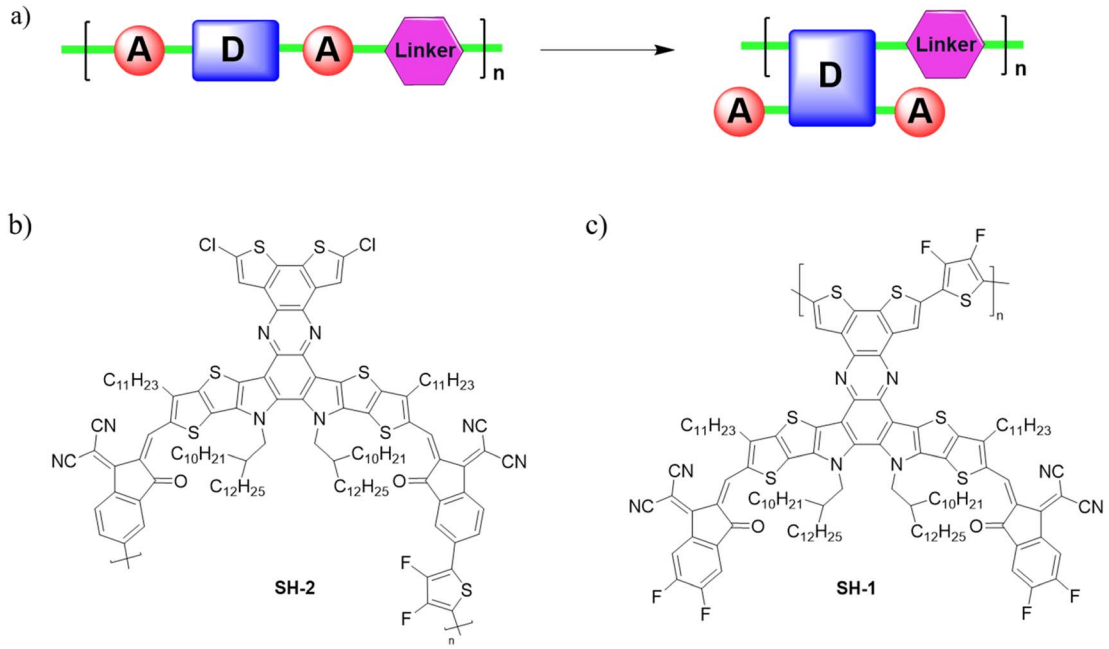

Fig. 1 (a) Diagram of the molecular design strategy. Chemical structure of (b) SH-2 and (c) SH-1.

deficient property of the end groups in the initial SMAs will be firstly changed after polymerization since one of the chemical modification sites with halogen atoms will be occupied to connect the end groups and linkers. Therefore, there is less chance to tune the property of polymer acceptors. (3) Regional isomerism problems:[25,35] in the polymerization strategy *via* the end groups, brominated 1,1-dicyanomethylene-3-indanone (IC) is the essential unit. However, the brominated IC unit is usually a mixture of two isomers with similar polarities, which is difficult to purify and leads to different configurations of the target polymer acceptors.[25]

To address the above issue, based on the polymerization SMA strategy, herein, we propose an alternative approach for designing polymer acceptors with grafted small molecule acceptor units (Fig. 1a). The rationale is as follows: (1) freeing the end groups of SMAs to facilitate the end group packing, which will be beneficial for electron transport; (2) formation of extended conjugation and double charge transport channels; (3) enriching the chemical modification sites and giving more chance to fine tune the optical and electrochemical properties of polymer acceptors. Following the above strategy, we designed and synthesized a polymer acceptor named **SH-1** with grafted SMA units. For comparison, a corresponding polymer acceptor **SH-2** was synthesized following the conventional polymerization way through the end groups and linkers. With PM6 as the donor polymer, **SH-1**-based all-PSC achieved a PCE of 14.14%, much better than that of the **SH-2**-based device with an efficiency of 6.55%. This work provides an alternative pathway to construct polymer acceptors based on the polymerization SMA strategy, demonstrating great potential for achieving higher efficiency all-PSCs through the delicate design of both SMA building blocks and linker groups.

2. Results and discussion

The synthetic routes of **SH-1** and **SH-2** are displayed in Scheme S1,† and the detailed synthesis procedures are provided in the ESI.† The average molecular weight (M_n) and polydispersity index (PDI) of **SH-1** are 14.8 kDa and 1.46, respectively. **SH-2** gave a similar M_n of 15.2 kDa and a broader polydispersity index of 1.97 (Fig. S1†). The UV-vis absorption spectra of **SH-1** and **SH-2** are shown in Fig. 2a. In CF solution, **SH-1** and **SH-2** show the maximum absorption (λ_{max}) peaks located at 778 and 792 nm, respectively. The blue shifted absorption of **SH-1** mainly comes from its weaker intramolecular charge transfer (ICT). Compared with their solution absorptions, the as-cast solid films of **SH-1** and **SH-2** display red-shifted peak absorptions by 12 and 8 nm, respectively, indicating a stronger aggregation tendency in the solid film for polymer acceptor **SH-1** with the grafted SMA unit. The optical bandgaps ($E_g o^{pt}$) calculated from the thin-film absorption edges of **SH-1** and **SH-2** are 1.45 and 1.38 eV, respectively. Furthermore, the temperature-dependent absorption spectra of the two polymer acceptors are studied. As shown in Fig. 1b and c, **SH-1** shows a smaller blue shifting of absorption peaks (~7 nm) than **SH-2** (~10 nm) with increasing the temperature from 10 to 100 °C, suggesting that **SH-1** exhibits more compact intermolecular stacking. The energy levels of the two acceptor films were investigated by electrochemical cyclic voltammetry (CV). From the onset reduction and oxidation potentials of the CV curves (Fig. S2†), the highest occupied molecular orbital (HOMO) level and the lowest unoccupied molecular orbit (LUMO) energy levels were estimated to be −5.68 and −3.69 eV for **SH-1**, −5.64 and −3.76 eV for **SH-2** (Fig. 2d, Table 1). Compared with **SH-2**, **SH-1** has a lower HOMO level, higher LUMO level and thus slightly increased bandgap.

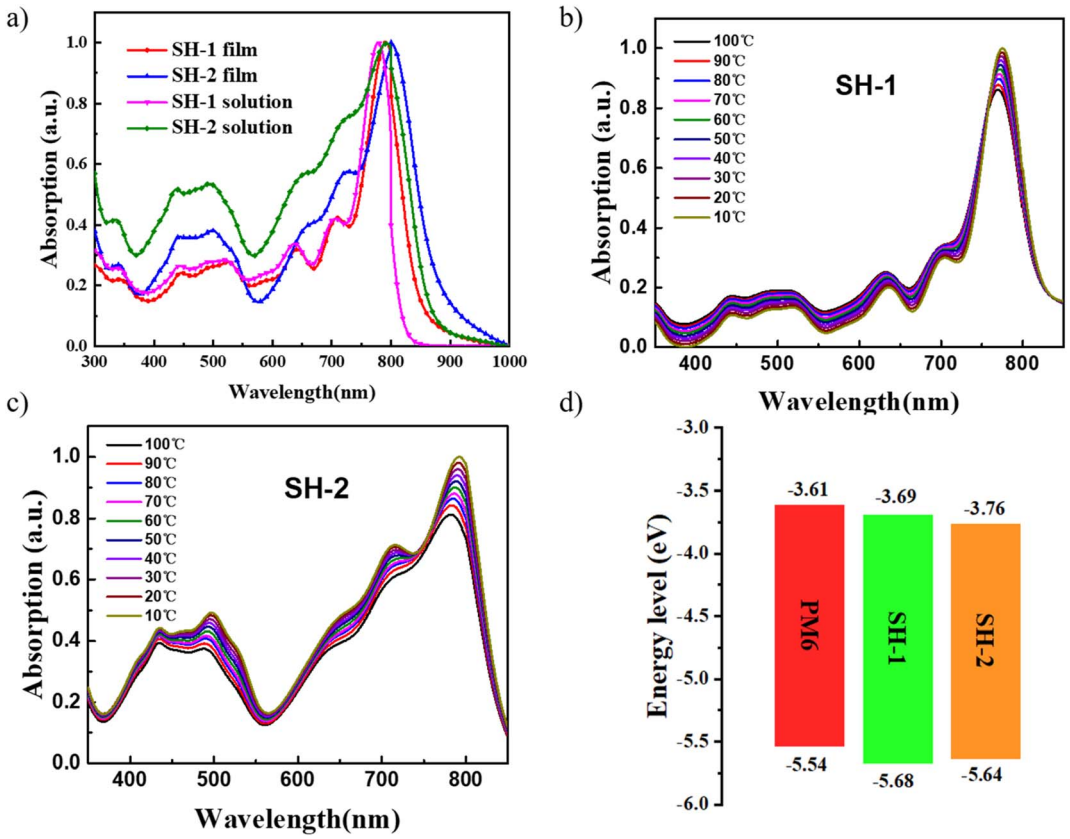

Fig. 2 (a) UV-vis absorption spectra of SH-1 and SH-2. Variable-temperature UV-vis absorption spectra of (b) SH-1 and (c) SH-2. (d) Energy levels of PM6, SH-1 and SH-2.

Table 1 The optical and electrochemical properties of SH-1 and SH-2

Comp.	λ_{max}^{sol} (nm)	λ_{max}^{film} (nm)	HOMO (eV)	LUMO (eV)	λ_{onset}^{film} (nm)	$E_g o^{pt}$ (eV)	E_g^{cv} (eV)
SH-1	778	790	−5.68	−3.69	855	1.45	1.99
SH-2	792	800	−5.64	−3.76	896	1.38	1.88

With the matched energy levels and complementary absorptions with the two polymer acceptors, the wide-bandgap polymer PM6 was selected as the donor to fabricate all-PSCs using the device structure ITO/PEDOT:PSS/active layers/PNDIT-F3N/Ag (Fig. 3a). The details of device fabrication are presented in the ESI† and the detailed device data are listed in Tables S1–S4.† The current density–voltage (J–V) curves of the optimized devices are illustrated in Fig. 3b, and the corresponding photovoltaic parameters are listed in Table 2. The optimal PM6:**SH-1**-based device achieved a PCE of 14.13% with a V_{oc} of 0.979 V, a J_{sc} of 21.03 mA cm^{-2}, and an FF of 68.67%. In contrast, the optimal device of PM6:**SH-2** showed a PCE of 6.55% with a V_{oc} of 0.908 V, a J_{sc} of 12.87 mA cm^{-2}, and an FF of 55.94%. The external quantum efficiency (EQE) curves of the two devices are illustrated in Fig. 3c. The PM6:**SH-1**-based all-PSC exhibits substantially higher EQE compared with PM6:**SH-2**, thereby achieving a much larger integrated current density of 20.50 mA cm^{-2} for PM6:**SH-1** than that of PM6:**SH-2** with a value of 12.63 mA cm^{-2}.

To clarify the variation of photovoltaic parameters of the two all-PSCs, the properties of the charge transport, exciton dissociation and charge generation of the two devices were investigated. The charge mobilities of the two blend films were studied using the space-charge-limited current (SCLC) method.[36] As shown in Fig. 4a, the PM6:**SH-1**-based device exhibits higher electron/hole mobilities (2.16×10^{-4}/2.93×10^{-4} cm^{-2} V^{-1} s^{-1}) compared with the PM6:**SH-2**-based device (1.46×10^{-4}/1.88×10^{-4} cm^{-2} V^{-1} s^{-1}). The enhanced μ_h and μ_e are beneficial to promote charge transport and contribute to the higher FF and J_{sc} of the PM6:**SH-1**-based device. Furthermore, in order to investigate the exciton dissociation and charge generation properties, the dependence of photocurrent density (J_{ph}) *versus* effective voltage (V_{eff}) was measured for the two devices (Fig. 4b). The exciton dissociation probability (P_{diss}) is calculated from J_{ph} under the short-circuit condition divided by the saturated photocurrent density (J_{sat}).[37] The PM6:**SH-1**-based device shows a P_{diss} of 88.7%, which is much higher than the PM6:**SH-2**-based device (54.6%), demonstrating the highly efficient exciton

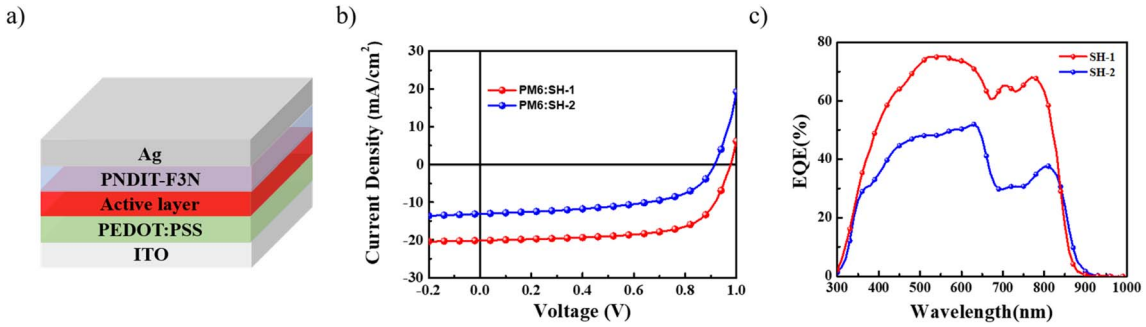

Fig. 3 (a) Photovoltaic device architecture. (b) *J*–*V* and (c) EQE curves of the optimized device.

Table 2 The optimal photovoltaic parameters of PM6:**SH-1** and PM6:**SH-2**-based devices under AM 1.5 G illumination (100 mW cm^{-2})

Active layer	V_{oc} (V)	J_{sc} (mA cm^{-2})	FF (%)	PCE[a] (%)
PM6:**SH-1**	0.979 (0.981 ± 0.003)	21.03 (20.37 ± 0.58)	68.67 (68.81 ± 1.04)	14.14 (13.63 ± 0.19)
PM6:**SH-2**	0.908 (0.910 ± 0.002)	12.87 (12.26 ± 0.59)	55.94 (54.94 ± 0.96)	6.55 (6.15 ± 0.38)

[a] Statistical and optimal results are listed in and outside of the parentheses, respectively, and the average parameters were calculated from 10 independent cells.

dissociation in the device based on PM6:**SH-1**. To study the behaviour of charge recombination of the two devices, we measured the J_{sc} and V_{oc} of solar cells by varying the light-intensity (P_{light}). As shown in Fig. 4c, the plots of P_{light} *versus* J_{sc} ($J_{sc} \propto P^{\alpha}$, where the exponent α being close to 1 reflects weak bimolecular recombination[38–42]) were measured to be 0.975 and

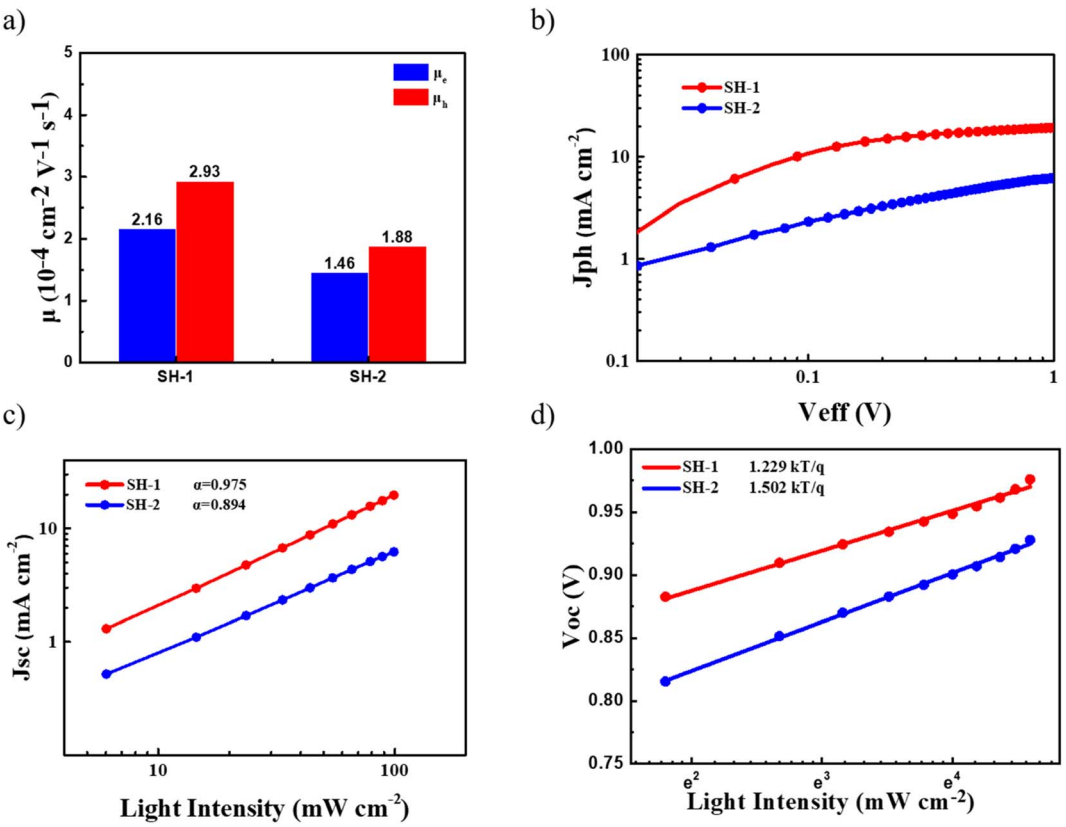

Fig. 4 (a) The carrier transport properties of PM6:**SH-1** or **SH-2**. (b) J_{ph} *versus* V_{eff} characteristics, (c) J_{sc} and (d) V_{oc} *versus* light intensity of the optimized devices.

0.894 for PM6:**SH-1** and PM6:**SH-2**-based devices, respectively. In view that the two devices had a similar μ_h/μ_e ratio of 1.35 and 1.29, the above α value results indicate that the PM6:**SH-1**-based device exhibited a weaker bimolecular recombination and suppressed recombination compared with those of the PM6:**SH-2**-based device.[43] Fig. 4d shows the relationship between the light intensity and V_{oc}. The slope of V_{oc} *versus* the natural logarithm of P_{light} can reflect the types of charge recombination in the device.[44] The slope is calculated to be $1.229kT/q$ and $1.502kT/q$ for PM6:**SH-1** and PM6:**SH-2**-based devices, indicating that the PM6:**SH-1**-based device had less bulk and surface trap-assisted recombination than the PM6:**SH-2**-based device.[45,46]

As it is known, the charge transfer/transport processes and photovoltaic performances are closely related to the morphology of active layer blend films. Therefore, atomic force microscopy (AFM) was used to visualize the surface morphologies of PM6:**SH-1** and PM6:**SH-2** blend films. As illustrated in Fig. 5, the two blend films show clearly different morphologies. The root-mean-square roughness (R_q) values are 3.65 and 10.2 nm for PM6:**SH-1** and PM6:**SH-2** blend films, respectively. Compared with the **SH-2**-based blend film, the PM6:**SH-1** film gives a much smoother surface morphology. Moreover, the PM6:**SH-1** blend film has a more featured interpenetrating structure, which is favourable for the exciton separation and charge transport. In contrast, the PM6:**SH-2** blend film is more inclined to aggregate and results in a large phase separation. The neat films of **SH-1** and **SH-2** are also investigated (Fig. S3†). The **SH-2** film also shows a rough surface distinguishing from the smooth film of **SH-1**, which is consistent with the blend film results.

Grazing incidence wide-angle X-ray scattering (GIWAXS) was used to further investigate the impact of the molecular packing motifs and microstructure for the two acceptors. Compared with **SH-2**, **SH-1** neat film shows intense π–π stacking with a distance of 3.86 Å (Fig. S4, Table S5†), demonstrating that the polymer acceptor **SH-1** with the grafted SMA unit favours the intermolecular packing. As shown in Fig. 5c and f, PM6:**SH-1** and PM6:**SH-2** blend films all show the clear stacking peaks in the out of plane (OOP) direction, indicating the face-on dominant orientations. In comparison with the neat films, the two blend films exhibit enhanced and shifted (010) peaks at 1.67 $Å^{-1}$ with a d spacing of 3.76 Å for the PM6:**SH-1** blend film and 1.65 $Å^{-1}$ with a d spacing of 3.81 Å for the PM6:**SH-2** blend film (Table S5†). As listed in Table S6,† the crystal coherence length (CCL) of the PM6:**SH-1** film is 34.48 Å, larger than that of the PM6:**SH-2** film (28.56 Å), suggesting the more ordered molecular packing for the PM6:**SH-1** film.[47] The more compact intermolecular stacking of PM6:**SH-1** should be attributed to its more planar conjugated backbone and the efficient packing of the end groups, which is beneficial for charge transport in the photovoltaic devices, consistent with the SCLC and AFM results.[48]

Notably, the devices based on PM6:**SH-1** and PM6:**SH-2** both show high V_{oc} (>0.9 V), especially PM6:**SH-1**. To investigate the reason behind it, the detailed E_{loss} analysis was conducted. The E_{loss} of the devices were calculated to be 0.522 eV (PM6:**SH-1**) and 0.529 eV (PM6:**SH-2**) following the equation:[49]

$$E_{loss} = E_{gap} - qV_{oc}$$

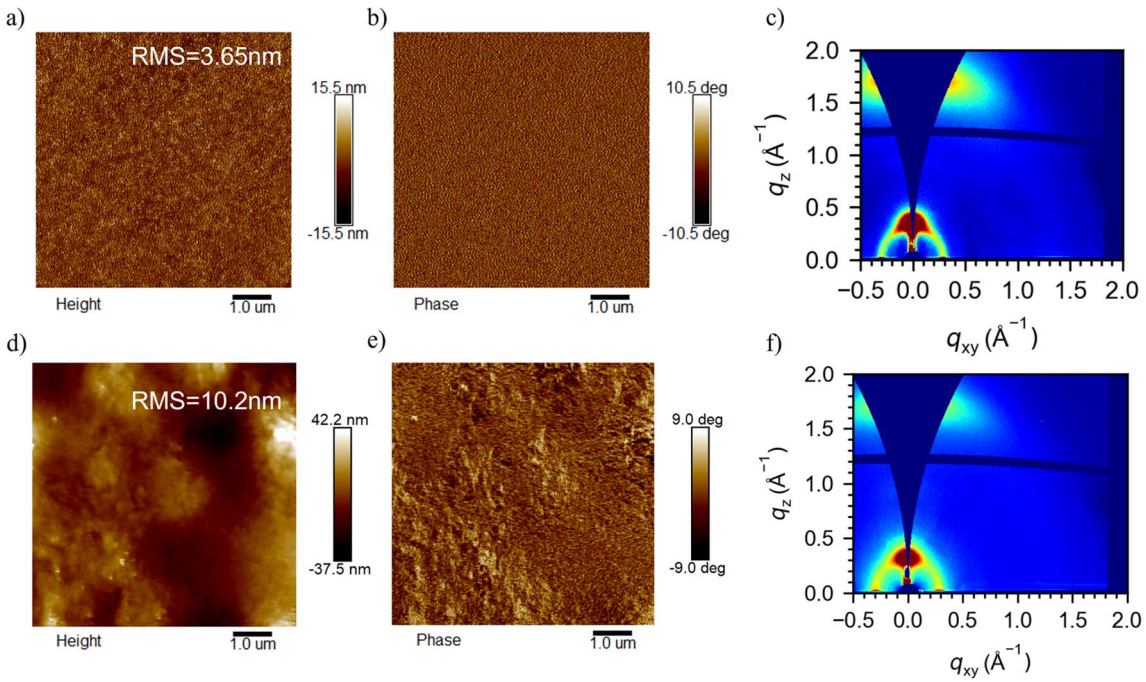

Fig. 5 (a) AFM height image, (b) AFM phase image and (c) GIWAXS pattern for the PM6:**SH-1** blend film. (d) AFM height image, (e) AFM phase image and (f) GIWAXS pattern for the PM6:**SH-2** blend film.

Table 3 Measured voltage losses for the optimized devices

Devices	E_g [eV]	V_{OC}^{SQ} [V]	ΔE_1 [eV]	V_{OC}^{rad} [V]	ΔE_2 [eV]	ΔE_3 [eV]	E_{loss} [eV]
PM6:**SH-1**	1.501	1.232	0.269	1.182	0.050	0.203	0.522
PM6:**SH-2**	1.437	1.172	0.265	1.132	0.040	0.224	0.529

The E_{gap} used in the equation was estimated by the intersections between the absorption and emission (Fig. S5†). Next, based on the Shockley–Queisser (SQ) theory, the detailed E_{loss} components were investigated.[50] According to this theory, the E_{loss} can be divided into three parts: $E_{loss} = \Delta E_1 + \Delta E_2 + \Delta E_3$, where ΔE_1 is the radiative recombination loss above the bandgap, ΔE_2 is the radiative recombination loss below the bandgap,[51] ΔE_3 is the nonradiative energy loss. As summarized in Table 3, the devices show similar ΔE_1 value of 0.269 eV and 0.265 eV calculated from the equation as follows:

$$\Delta E_1 = E_{gap} - qV_{OC}^{SQ}$$

The value of ΔE_1 is comparable with other typical OSCs. Calculated from the Fourier transform photocurrent spectroscopy (FTPS) and EL spectroscopy, the device gave the V_{OC}^{rad} value and then we can achieve the ΔE_2 following the equation:

$$\Delta E_2 = qV_{OC}^{SQ} - qV_{OC}^{rad}$$

The third part ΔE_3, also named non-radiative combination energy loss, is calculated from the EQE_{EL} (Fig. S6†) following the equation:[52]

$$\Delta E_3 = -kT \ln EQE_{EL}$$

Clearly, both devices exhibit low E_{loss}, comparable with the high-efficiency state of the art devices. The limit of ΔE_3 in OSCs is reported to be defined by the photoluminescence efficiencies of the low band gap component, *i.e.*, the acceptor in the active layer for the typical non-fullerene based OSCs.[53] As shown in Fig. S7,† the neat film of **SH-1** demonstrates a photoluminescence quantum yield (PLQY) of 5.67%, higher than that of **SH-2** with the value of 5.44% (Fig. S8†). The high PLQY of **SH-1** might originate from their enhanced J-aggregation in the solid films, which has proved to favor high luminescence efficiencies.[54] As a result, the PM6:**SH-1**-based device gives a slightly lower E_{loss} than the PM6:**SH-2**-based device primarily due to its lower ΔE_3.

3. Conclusions

In summary, we have proposed a strategy for designing polymer acceptors with grafted SMA units *via* the polymerization through central building blocks of SMAs and linkers. This design strategy can not only free the end groups to facilitate the effective end group packing similar to SMAs but also favor extended conjugation and double charge transport channel, which can enhance π–π interactions and facilitate charge transport. With this strategy, the obtained polymer acceptor **SH-1** exhibits more compact and ordered intermolecular packing in both neat and blended films compared with **SH-2** synthesized by copolymerizing *via* SMA end groups and linkers. With more efficient exciton dissociation, facilitated charge transport, and suppressed recombination, the all-PSC device based on PM6:**SH-1** showed a PCE over 14%, substantially higher than that of the PM6:**SH-2** based device with an efficiency of 6.55%. These results indicate that the design strategy of polymer acceptors with grafted small molecule acceptors is an efficient way to construct high performance all PSCs. It is believed that higher efficiency polymer acceptors can be designed using the above strategy through the delicate regulation of both the central building block and linker groups.

Conflicts of interest

There are no conflicts of interest to declare.

Acknowledgements

The authors thank Yu Chen at Beijing Synchrotron Radiation Facility, Institute of High Energy Physics for performing GIWAXS measurement. The author gratefully acknowledges the financial support from MoST of China (2022YFB4200400, 2019YFA0705900) and NSFC (52025033, 52173010 and 21935007).

Notes and references

1 J. Yuan, Y. Zhang, L. Zhou, G. Zhang, H.-L. Yip, T.-K. Lau, X. Lu, C. Zhu, H. Peng, P. A. Johnson, M. Leclerc, Y. Cao, J. Ulanski, Y. Li and Y. Zou, *Joule*, 2019, **3**, 1140–1151.
2 L. Meng, Y. Zhang, X. Wan, C. Li, X. Zhang, Y. Wang, X. Ke, Z. Xiao, L. Ding, R. Xia, H.-L. Yip, Y. Cao and Y. Chen, *Science*, 2018, **361**, 1094–1098.
3 A. J. Gillett, A. Privitera, R. Dilmurat, A. Karki, D. Qian, A. Pershin, G. Londi, W. K. Myers, J. Lee, J. Yuan, S.-J. Ko, M. K. Riede, F. Gao, G. C. Bazan, A. Rao, T.-Q. Nguyen, D. Beljonne and R. H. Friend, *Nature*, 2021, **597**, 666–671.
4 X. Du, T. Heumueller, W. Gruber, O. Almora, A. Classen, J. Qu, F. He, T. Unruh, N. Li and C. J. Brabec, *Adv. Mater.*, 2020, **32**, 1908305.
5 X. Ke, L. Meng, X. Wan, M. Li, Y. Sun, Z. Guo, S. Wu, H. Zhang, C. Li and Y. Chen, *J. Mater. Chem. A*, 2020, **8**, 9726–9732.
6 L. Xie, W. Song, J. Ge, B. Tang, X. Zhang, T. Wu and Z. Ge, *Nano Energy*, 2021, **82**, 105770.
7 L. Ye, K. Weng, J. Xu, X. Du, S. Chandrabose, K. Chen, J. Zhou, G. Han, S. Tan, Z. Xie, Y. Yi, N. Li, F. Liu,

J. M. Hodgkiss, C. J. Brabec and Y. Sun, *Nat. Commun.*, 2020, **11**, 6005.
8 H. Chen, Y. Zou, H. Liang, T. He, X. Xu, Y. Zhang, Z. Ma, J. Wang, M. Zhang, Q. Li, C. Li, G. Long, X. Wan, Z. Yao and Y. Chen, *Sci. China: Chem.*, 2022, **65**, 1362–1373.
9 X. Wan, C. Li, M. Zhang and Y. Chen, *Chem. Soc. Rev.*, 2020, **49**, 2828–2842.
10 Y. Cui, Y. Xu, H. Yao, P. Bi, L. Hong, J. Zhang, Y. Zu, T. Zhang, J. Qin, J. Ren, Z. Chen, C. He, X. Hao, Z. Wei and J. Hou, *Adv. Mater.*, 2021, **33**, 2102420.
11 W. Gao, F. Qi, Z. Peng, F. R. Lin, K. Jiang, C. Zhong, W. Kaminsky, Z. Guan, C.-S. Lee, T. J. Marks, H. Ade and A. K. Y. Jen, *Adv. Mater.*, 2022, **34**, 2202089.
12 D. Li, N. Deng, Y. Fu, C. Guo, B. Zhou, L. Wang, J. Zhou, D. Liu, W. Li, K. Wang, Y. Sun and T. Wang, *Adv. Mater.*, 2023, **35**, 2208211.
13 L. Meng, H. Liang, G. Song, M. Li, Y. Huang, C. Jiang, K. Zhang, F. Huang, Z. Yao, C. Li, X. Wan and Y. Chen, *Sci. China: Chem.*, 2023, **66**, 808–815.
14 Y. Wei, Z. Chen, G. Lu, N. Yu, C. Li, J. Gao, X. Gu, X. Hao, G. Lu, Z. Tang, J. Zhang, Z. Wei, X. Zhang and H. Huang, *Adv. Mater.*, 2022, **34**, 2204718.
15 L. Zhan, S. Li, Y. Li, R. Sun, J. Min, Z. Bi, W. Ma, Z. Chen, G. Zhou, H. Zhu, M. Shi, L. Zuo and H. Chen, *Joule*, 2022, **6**, 662–675.
16 G. Wang, F. S. Melkonyan, A. Facchetti and T. J. Marks, *Angew. Chem., Int. Ed.*, 2019, **58**, 4129–4142.
17 J. Yang, B. Xiao, A. Tang, J. Li, X. Wang and E. Zhou, *Adv. Mater.*, 2019, **31**, 1804699.
18 Z.-G. Zhang and Y. Li, *Angew. Chem., Int. Ed.*, 2021, **60**, 4422–4433.
19 M. Kataria, H. D. Chau, N. Y. Kwon, S. H. Park, M. J. Cho and D. H. Choi, *ACS Energy Lett.*, 2022, **7**, 3835–3854.
20 Y. Cai, C. Xie, Q. Li, C. Liu, J. Gao, M. H. Jee, J. Qiao, Y. Li, J. Song, X. Hao, H. Y. Woo, Z. Tang, Y. Zhou, C. Zhang, H. Huang and Y. Sun, *Adv. Mater.*, 2023, **35**, 2208165.
21 Z.-G. Zhang, Y. Yang, J. Yao, L. Xue, S. Chen, X. Li, W. Morrison, C. Yang and Y. Li, *Angew. Chem., Int. Ed.*, 2017, **56**, 13503–13507.
22 J. Song, C. Li, J. Qiao, C. Liu, Y. Cai, Y. Li, J. Gao, M. H. Jee, X. Hao, H. Y. Woo, Z. Tang, H. Yan and Y. Sun, *Matter*, 2023, **6**, 1542–1554.
23 T. Zhang, Y. Xu, H. Yao, J. Zhang, P. Bi, Z. Chen, J. Wang, Y. Cui, L. Ma, K. Xian, Z. Li, X. Hao, Z. Wei and J. Hou, *Energy Environ. Sci.*, 2023, **16**, 1581–1589.
24 X. Yang, R. Sun, Y. Wang, M. Chen, X. Xia, X. Lu, G. Lu and J. Min, *Adv. Mater.*, 2023, **35**, 2209350.
25 Z. Luo, T. Liu, R. Ma, Y. Xiao, L. Zhan, G. Zhang, H. Sun, F. Ni, G. Chai, J. Wang, C. Zhong, Y. Zou, X. Guo, X. Lu, H. Chen, H. Yan and C. Yang, *Adv. Mater.*, 2020, **32**, 2005942.
26 G. Sun, X. Jiang, X. Li, L. Meng, J. Zhang, S. Qin, X. Kong, J. Li, J. Xin, W. Ma and Y. Li, *Nat. Commun.*, 2022, **13**, 5267.
27 L. Zhou, L. Meng, J. Zhang, S. Qin, J. Guo, X. Li, X. Xia, X. Lu and Y. Li, *Macromolecules*, 2022, **55**, 4420–4428.
28 Q. Fan, W. Su, S. Chen, W. Kim, X. Chen, B. Lee, T. Liu, U. A. Méndez-Romero, R. Ma, T. Yang, W. Zhuang, Y. Li, Y. Li, T.-S. Kim, L. Hou, C. Yang, H. Yan, D. Yu and E. Wang, *Joule*, 2020, **4**, 658–672.
29 S. Ma, H. Zhang, K. Feng and X. Guo, *Chem.–Eur. J.*, 2022, **28**, e202200222.
30 H. Yao, F. Bai, H. Hu, L. Arunagiri, J. Zhang, Y. Chen, H. Yu, S. Chen, T. Liu, J. Y. L. Lai, Y. Zou, H. Ade and H. Yan, *ACS Energy Lett.*, 2019, **4**, 417–422.
31 J. Cao, L. Yi and L. Ding, *J. Semicond.*, 2022, **43**, 030202.
32 W. Zhu, A. P. Spencer, S. Mukherjee, J. M. Alzola, V. K. Sangwan, S. H. Amsterdam, S. M. Swick, L. O. Jones, M. C. Heiber, A. A. Herzing, G. Li, C. L. Stern, D. M. DeLongchamp, K. L. Kohlstedt, M. C. Hersam, G. C. Schatz, M. R. Wasielewski, L. X. Chen, A. Facchetti and T. J. Marks, *J. Am. Chem. Soc.*, 2020, **142**, 14532–14547.
33 Y. Zou, H. Chen, X. Bi, X. Xu, H. Wang, M. Lin, Z. Ma, M. Zhang, C. Li, X. Wan, G. Long, Y. Zhaoyang and Y. Chen, *Energy Environ. Sci.*, 2022, **15**, 3519–3533.
34 H. Yu, Y. Wang, H. K. Kim, X. Wu, Y. Li, Z. Yao, M. Pan, X. Zou, J. Zhang, S. Chen, D. Zhao, F. Huang, X. Lu, Z. Zhu and H. Yan, *Adv. Mater.*, 2022, **34**, 2200361.
35 C. He, Z. Chen, T. Wang, Z. Shen, Y. Li, J. Zhou, J. Yu, H. Fang, Y. Li, S. Li, X. Lu, W. Ma, F. Gao, Z. Xie, V. Coropceanu, H. Zhu, J.-L. Bredas, L. Zuo and H. Chen, *Nat. Commun.*, 2022, **13**, 2598.
36 Y. Shen, A. R. Hosseini, M. H. Wong and G. G. Malliaras, *ChemPhysChem*, 2004, **5**, 16–25.
37 C. M. Proctor, M. Kuik and N. Thuc-Quyen, *Prog. Polym. Sci.*, 2013, **38**, 1941–1960.
38 D. Credgington, F. C. Jamieson, B. Walker, N. Thuc-Quyen and J. R. Durrant, *Adv. Mater.*, 2012, **24**, 2135–2141.
39 L. J. A. Koster, V. D. Mihailetchi, H. Xie and P. W. M. Blom, *Appl. Phys. Lett.*, 2005, **87**, 203502.
40 A. K. K. Kyaw, D. H. Wang, C. Luo, Y. Cao, T.-Q. Nguyen, G. C. Bazan and A. J. Heeger, *Adv. Energy Mater.*, 2014, **4**, 1301469.
41 C. M. Proctor, C. Kim, D. Neher and N. Thuc-Quyen, *Adv. Funct. Mater.*, 2013, **23**, 3584–3594.
42 P. Schilinsky, C. Waldauf and C. J. Brabec, *Appl. Phys. Lett.*, 2002, **81**, 3885–3887.
43 L. J. A. Koster, V. D. Mihailetchi, H. Xie and P. W. M. Blom, *Appl. Phys. Lett.*, 2005, **87**, 203502.
44 X. Gong, M. Tong, F. G. Brunetti, J. Seo, Y. Sun, D. Moses, F. Wudl and A. J. Heeger, *Adv. Mater.*, 2011, **23**, 2272–2277.
45 V. V. Brus, *Org. Electron.*, 2016, **29**, 1–6.
46 J. Vollbrecht and V. V. Brus, *Org. Electron.*, 2020, **86**, 105905.
47 Z. Zhang, Y. Li, G. Cai, Y. Zhang, X. Lu and Y. Lin, *J. Am. Chem. Soc.*, 2020, **142**, 18741–18745.
48 T. Liu, Y. Zhang, Y. Shao, R. Ma, Z. Luo, Y. Xiao, T. Yang, X. Lu, Z. Yuan, H. Yan, Y. Chen and Y. Li, *Adv. Funct. Mater.*, 2020, **30**, 2000456.
49 K. Vandewal, J. Benduhn and V. C. Nikolis, *Sustainable Energy Fuels*, 2018, **2**, 538–544.
50 U. Rau, B. Blank, T. C. M. Müller and T. Kirchartz, *Phys. Rev. Appl.*, 2017, **7**, 044016.
51 S. Chen, Y. Wang, L. Zhang, J. Zhao, Y. Chen, D. Zhu, H. Yao, G. Zhang, W. Ma, R. H. Friend, P. C. Y. Chow, F. Gao and H. Yan, *Adv. Mater.*, 2018, **30**, 1804215.

52 U. Rau, *Phys. Rev. B: Condens. Matter Mater. Phys.*, 2007, **76**, 085303.
53 X.-K. Chen, D. Qian, Y. Wang, T. Kirchartz, W. Tress, H. Yao, J. Yuan, M. Hülsbeck, M. Zhang, Y. Zou, Y. Sun, Y. Li, J. Hou, O. Inganäs, V. Coropceanu, J.-L. Bredas and F. Gao, *Nat. Energy*, 2021, **6**, 799–806.
54 N. J. Hestand and F. C. Spano, *Chem. Rev.*, 2018, **118**, 7069–7163.